## Title
Water and Thermal Management in Solid-Polymer-Electrolyte Fuel Cells



## Journal
Journal of the Electrochemical Society, 140(5)

## Authors
Fuller, T.F.
Newman, J.

## Publication Date
1992-08-01

LBL-32644
UC-334
Preprint

# Lawrence Berkeley Laboratory
UNIVERSITY OF CALIFORNIA

## Materials Sciences Division

Submitted to Journal of the Electrochemical Society

## Water and Thermal Management in Solid-Polymer-Electrolyte Fuel Cells

T.F. Fuller and J. Newman

August 1992



Prepared for the U.S. Department of Energy under Contract Number DE-AC03-76SF00098

## DISCLAIMER

UC-334

# Water and Thermal Management in Solid-polymer-electrolyte Fuel Cells

Thomas F. Fuller and John Newman

Department of Chemical Engineering
University of California

and

Materials Sciences Division
Lawrence Berkeley Laboratory
University of California
Berkeley, California 94720

August 1992

This work was supported in part by the Assistant Secretary for Conservation and Renewable Energy, Office of Transportation Technologies, Electric and Hybrid Propulsion Division of the U. S. Department of Energy under Contract No. DE-AC03-76SF00098.

# Water and Thermal Management in Solid-polymer-electrolyte Fuel Cells

Thomas F. Fuller and John Newman

## Abstract

A mathematical model of transport in a solid-polymer-electrolyte fuel cell is presented. A two-dimensional membrane-electrode assembly is considered. Water management, thermal management, and utilization of fuel are examined in detail. Because the equilibrium sorption of water between the gas phase and the polymer-electrolyte depends strongly on temperature, water and thermal management are interrelated. The rate of heat removal is shown to be a critical parameter in the operation of these fuel cells.

## Introduction

As interest in electric vehicles increases, solid-polymer-electrolyte fuel cells are receiving renewed attention. Dramatic improvements in the performance of single, laboratory-scale cells with low platinum loading have been made over the last few years.[1,2] Because several interrelated processes occur simultaneously, the development of a mathematical model is critical to the design and scale-up of solid-polymer-electrolye fuel cells. In particular, understanding thermal effects, which are inseparable from the management of water in the polymer, is necessary to optimize the performance of these fuel cells.

One method of fabricating solid-polymer-electrolyte fuel cells is to hot-press two gas-diffusion electrodes onto a thin polymer membrane above its glass-transition temperature.[3] This is shown schematically in figure 1. Leddy and Vanderborgh[4] characterize the membrane-electrode interface and present a photomicrograph of the region. There are three phases present: a solid phase consisting of the porous graphite electrode and platinum catalyst, the solid polymer electrolyte, and a gas phase. Descriptions of gas-diffusion electrodes and corresponding models can be found in the literature.[5,6,7]

Nguyen *et al.*[8] raise mass- and heat-transfer design issues in polymer-electrolyte fuel cells, but by and large the subject has not been treated in the literature. Recently, Kimble and White[9] presented a detailed model of an alkaline fuel cell; solid-polymer-electrolyte fuel-cell models have been developed by Bernardi and Verbrugge[10,11,12] and by Springer *et al.*[13] In contrast to these, our model uses concentrated solution theory, treats the two-dimensional membrane-electrode

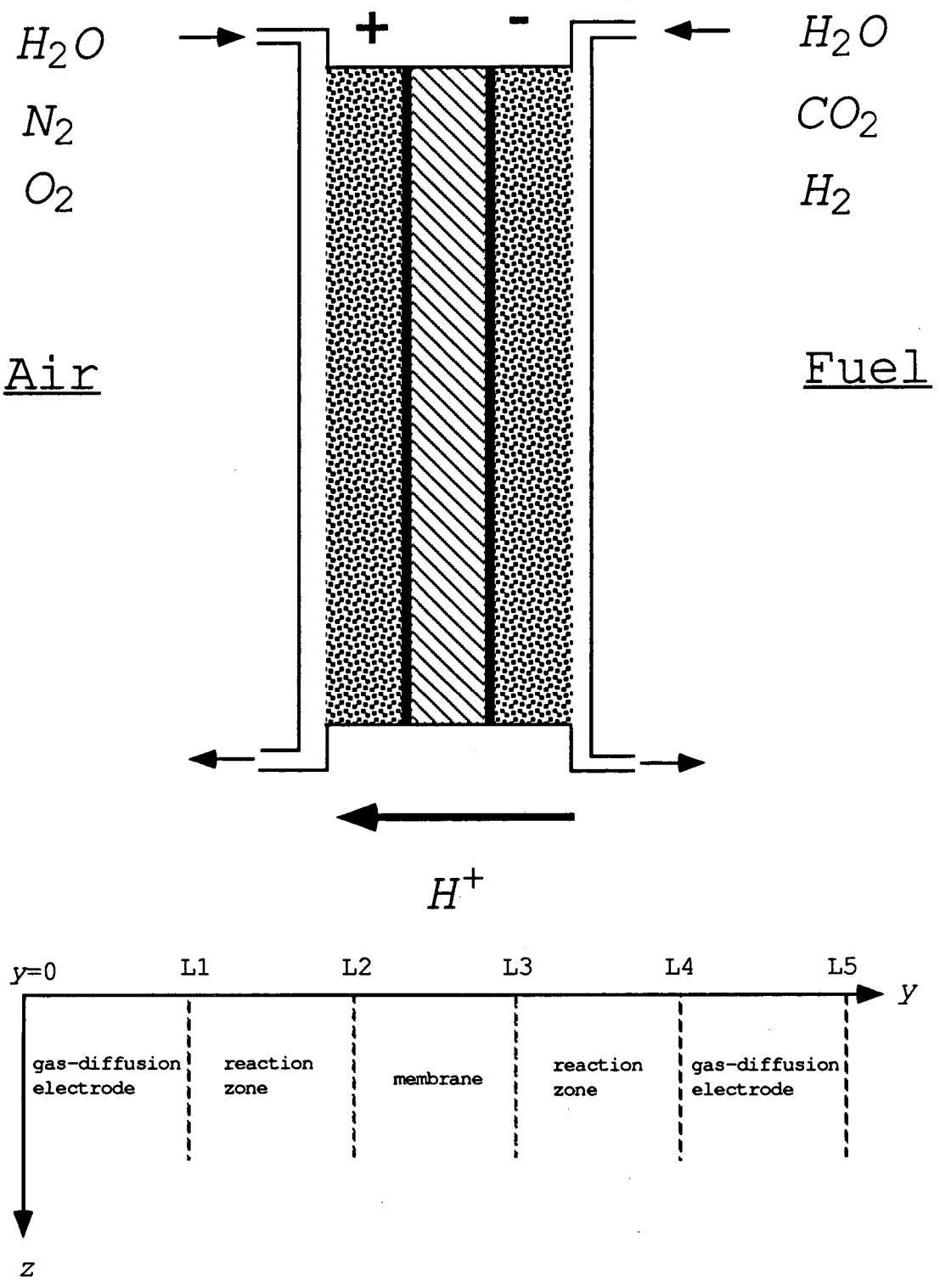


Figure 1. Membrane and electrode assembly. The five regions of the model are shown (not to scale).

assembly, and accounts for thermal effects.

We consider a membrane-electrode assembly operating at steady state on air and reformed methanol. The fuel and air streams are heated and humidified before entering their respective channels where they are consumed in electrochemical reactions. Hydrogen gas diffuses through the porous electrode and is oxidized on platinum catalyst sites at the anode in a three-phase region containing polymer electrolyte, gaseous reactants, and carbon matrix. Oxygen passes through the gas-diffusion electrodes to the cathode. At the cathode, the hydrogen ions react with oxygen at similar catalyst sites to form water. Water also absorbs into or evaporates from the membrane depending on its partial pressure.

After developing the model, we divide the analysis into three areas: 1) constant-temperature study of a unit cross section of the fuel cell, 2) water management in a membrane-electrode assembly at constant temperature with cocurrent flow of air and fuel, and 3) combined material and energy balance for the membrane-electrode assembly. We focus on the following water-management issues: the net transport of water, which must be supplied or recycled thereby reducing the efficiency of the cell, from the anode to the cathode; dehydration of the anode leading to high ohmic losses since the conductivity of the polymer electrolyte is a strong function of the degree of hydration, and flooding of the cathode.

It is common practice to saturate the inlet gases with water at a temperature higher than the operating temperature of the cell (producing a mist). Since water is produced at the cathode, it is not obvious that additional water need be supplied to the fuel cell. We hope to

elucidate when and why additional water might be needed to enhance the performance.

In addition, the utilization of hydrogen is an important factor in the optimization of these fuel cells. One could circumvent water and thermal management problems by increasing the flow rates of the gas streams. This will, however, affect the utilization of fuel, the net transport of water across the cell, and the efficiency of the fuel cell.

## Model

The cell sandwich is composed of five regions (see figure 1) and three phases. The species considered in the electrolyte are: the polymer with covalently bound sulfonic acid groups, hydrogen ions, and water. Transport in the polymer electrolyte is described with concentrated solution theory. The fundamental equation is

$$\mathbf{d}_i = \sum_{j \neq i}^{n} K_{ij}(\mathbf{v}_j - \mathbf{v}_i), \tag{1}$$

where $\mathbf{d}_i$ is the driving force for transport and $K_{ij}$'s are frictional coefficients. Equation 1 may be put in the form of the Stefan-Maxwell equation; for $n$ species,

$$\frac{c_i \nabla \mu_i}{RT} = \sum_{j \neq i}^{n} \frac{x_i J_j - x_j J_i}{c D_{ij}} , \tag{2}$$

where the molar flux is given by

$$J_i = c_i(\mathbf{v}_i - \mathbf{v}_{ref}) . \tag{3}$$

In developing equation 2, we introduced the molecular weight of the

polymer. However, the fundamental transport equations are independent of molecular weight, and this choice is somewhat arbitrary. We assumed the molecular weight of the polymer is equal to its equivalent weight. More details of the membrane-transport model and on the measurement of their transport properties are given by Fuller and Newman.[14,15,16]

There are three species in each gas stream: nitrogen, oxygen, and water vapor in the cathode; carbon dioxide, hydrogen, and water vapor in the anode. The Stefan-Maxwell equations can also be used to describe multicomponent diffusion of gases.[17] For convenience, the reference velocity is set to zero (that of the nondiffusing gases, carbon dioxide and nitrogen, and the polymer).

Equation 2 is combined with a material balance on species $i$,

$$\frac{\partial(\epsilon c_i)}{\partial t} = -\nabla \cdot \mathbf{J}_i + a j_{in}. \tag{4}$$

The pore-wall flux density of species $i$, $j_{in}$, is an average over the interfacial area between the gas-phase, electrode, and electrolyte. Because of the Gibbs-Duhem relationship, within each phase there are only $n-1$ independent equations of the form of equation (2).

The relationship among mole fractions in each phase is

$$\sum_{i=1}^{n} x_i = 1. \tag{5}$$

In the electrolyte, there is also the additional dependent variable, $\Phi$, the electrical potential. Newman discusses the various potentials we could use.[18] The electrochemical potential of each species is taken to

be

$$\nabla\mu_i = z_i F\nabla\Phi + RT\frac{\nabla x_i}{x_i} \quad . \tag{6}$$

Here the choice of molecular weight of the polymer implicitly affects the assumption for the activity. The equation of electroneutrality is

$$\sum_{i=1}^{n} z_i x_i = 0. \tag{7}$$

Within the reaction zones, we consider two chemical reactions:

$$\text{at the anode} \quad H_2 \rightleftarrows 2H^+ + 2e^-,$$

$$\text{at the cathode} \quad O_2 + 4H^+ + 4e^- \rightleftarrows 2H_2O,$$

$$\text{and} \quad H_2O_{(\ell)} \rightleftarrows H_2O_{(g)},$$

representing the absorption and evaporation of water from the membrane. Electron-transfer reactions are described by Butler-Volmer kinetics.

The problem is two dimensional, but the large aspect ratio allows us to consider transport only in the $y$ direction in the cell sandwich (see figure 1). Although this is not strictly correct, the expected improvements in results do not warrant the additional complexities of a more detailed two-dimensional model. We solve for transport in the $y$ direction at a given value of $z$ and integrate down the membrane-electrode assembly in the $z$ direction. The gas outside the gas-diffusion electrode is assumed to be of uniform composition in the $y$

direction. For large Péclet number, axial diffusion is neglected. A material balance on species $i$ in the anode gas channel, for example, gives

$$F_i - F_i^o = \int_0^z J_i|_{y=L5}\, dz. \tag{8}$$

References 18 and 19 discuss general energy balances for electrochemical systems. We assumed that temperature is a function of $z$ only. The work done by the system is $iV$. The rate of external heat transfer to the system may be expressed by

$$q = -h\,(T-T_A). \tag{9}$$

Application of the first law of thermodynamics to the fuel cell gives

$$-F_T\Delta H = \int_0^z h(T-T_A)dz + \int_0^z Vidz, \tag{10}$$

where $\Delta H$ is change in enthalpy per mole of gas and $F_T$ is the total molar flow rate of gas per unit width of the membrane-electrode assembly. Thus, the energy released by the overall chemical reaction is split among: electrical work, change in enthalpy (and hence temperature) of the flowing gas streams, and external heat transfer.

At each end of the fuel-cell assembly, $y$=0 and $y$=$L5$, the mole fractions of the gaseous species are determined from a material balance in the $z$ direction of the gas channel (see equation 8). At a phase boundary, the fluxes of the species within that phase are set to zero. At $L4$, for example, the fluxes of electrolyte species (water, hydrogen

ions, and membrane) are zero. Where there is a discontinuity in the porosity, the concentration and superficial fluxes are continuous. Therefore, at $L3$, the fluxes of gas species are set to zero, and the concentration and superficial fluxes of electrolyte species are matched. The solid carbon phase is assumed to be highly conductive. The potential of the anode is set to zero, and the potential of the cathode is specified and assumed constant, thereby setting the cell potential $V$ as a constant in $z$ and time.

The set of nonlinear, partial differential equations for the gas and electrolyte phases, together with the appropriate boundary conditions, are solved numerically. More details of this approach can be found in the work of Tribollet and Newman.[20] Since the effect of changes in individual properties (conductivity for example) seems evident, we do not attempt a parametric study. Instead, using the best available data, we examine the complex relationship between the operating conditions and transport in the fuel cell. Where possible, the parameters were obtained from our experimental results or from data available in the literature. The appendix summarizes the thermodynamic and kinetic data and the transport properties used in the simulation.

## Results and Discussion

*Unit cross section.* — First, we examine a unit cross section of the fuel cell. The temperature is fixed, and we specify the mole fractions of the gaseous species at the ends of the two gas-diffusion electrodes. The current-voltage curve for the conditions of table 1 is shown in figure 2. For all of the simulations the thickness of the gas diffusion electrodes was 360 $\mu$m, and the thickness of the reaction zone

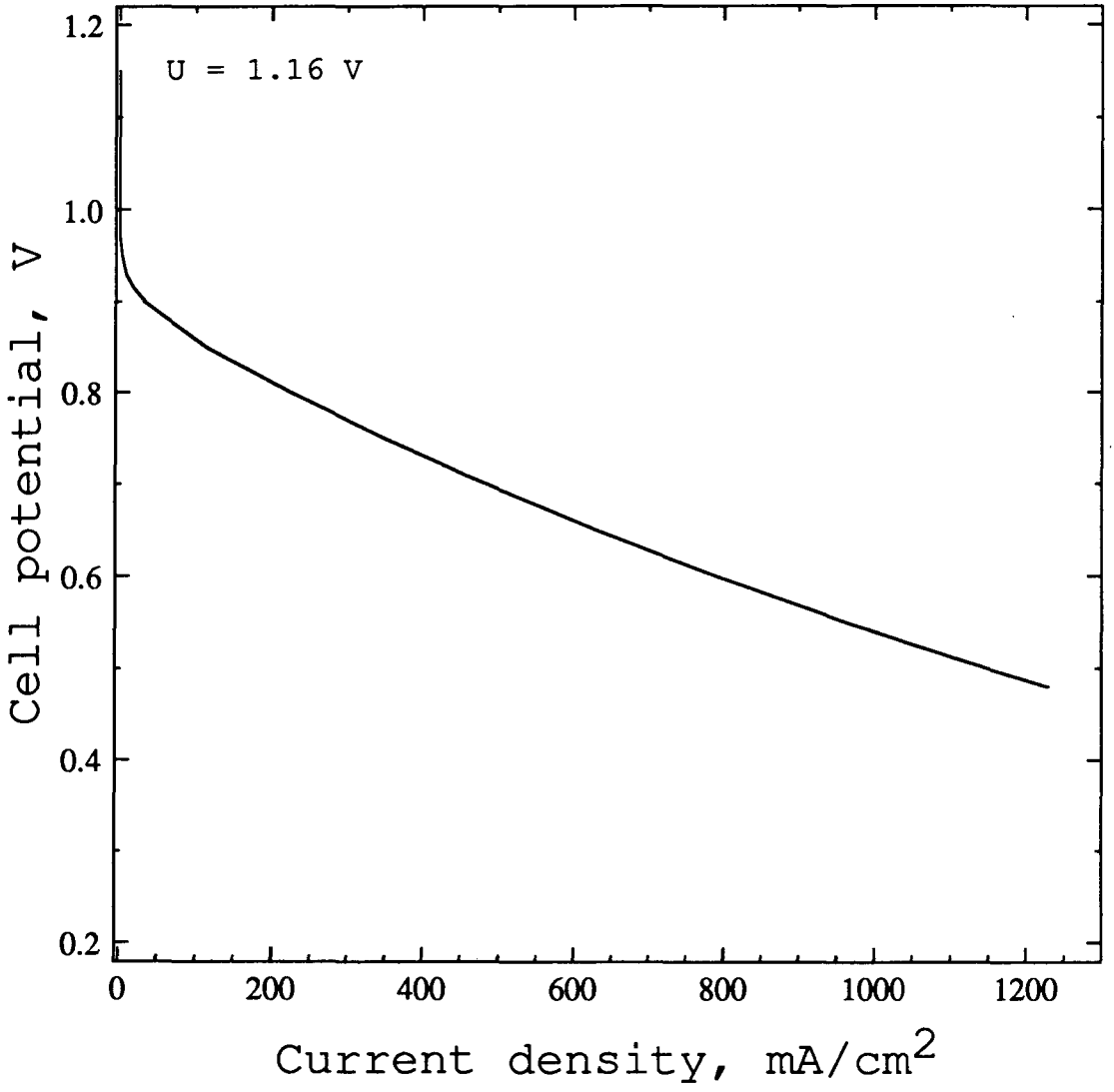


Figure 2. Cell potential versus current density for unit cell. Operating conditions are listed in table 1.

Table 1.
Gas composition at the boundaries.

| cathode-gas | | anode-gas | |
|---|---|---|---|
| $x_{H_2O}$ | 0.40 | $x_{H_2O}$ | 0.40 |
| $x_{N_2}$ | 0.48 | $x_{CO_2}$ | 0.15 |
| $x_{O_2}$ | 0.12 | $x_{H_2}$ | 0.45 |

| parameter | value |
|---|---|
| $T$ | 353.0 K |
| $L$ | 0.0175 cm |
| $p$ | 1.0 bar |
| $\epsilon_m$ | 0.20 |
| $\epsilon_g$ | 0.40 |

was 10 $\mu$m. At low current density, ohmic losses are small, and polarization at the cathode controls the cell potential. As the current density increases, ohmic losses grow, and the curve becomes roughly linear; in this region the slope is inversely proportional to the electrical conductivity. Because the water content, which determines the conductivity of the membrane, increases with current density, the curve is slightly concave upward (the water profiles in figure 3 will clarify this effect).

Ticianelli *et al.*[3] presented experimentally measured curves. They observed what appear to be mass-transfer limitations in experimental cells, a sharp drop in current density at low cell potentials. The model does not predict mass-transfer limitations in the gas-diffusion electrodes until current densities of about 5 A/cm$^2$. The model, however, does not include adsorption and mass transfer of hydrogen or oxygen in the water or polymer film, which could limit the current density. The mass-transfer limitations may also be the result of flooding; as the pores fill up with water, the volume fraction of the gas decreases, and

access to the catalyst may be restricted.

Figure 3 presents profiles of water content in the membrane at different current densities. $\lambda$ is the number of moles of water per sulfonic acid group. At the cathode, water is produced in stoichiometric proportion to the current; and with increasing current, more water is dragged from the anode. A concentration gradient builds up to counteract this electroosmotic drag.

As the current density grows, one observes an increase in the water content at the cathode and dehydration at the anode. Although the flux of water across the membrane is constant, because of variations in physical properties, the water profiles are not straight. There is little resistance to mass transfer in the gas phase or in the membrane; consequently, even at high current densities, dehydration of the anode is slight.

*Isothermal case.* — Next, we consider a two-dimensional membrane-electrode assembly (shown in figure 1), with cocurrent flow of air and fuel streams. The temperature is constant, but as the gas streams flow down the channels, fuel and oxygen are consumed, and water is produced at the cathode. Therefore, with the electrode potential fixed, the local current density and flux of water change. Here we account for these variations in the $z$ direction.

For the conditions given in table 2, figure 4 shows a two-dimensional water map in the membrane. $y$ is the dimension across the separator, and $z$ is along the length of the assembly. With increasing $z$, the partial pressure of water increases in the channel because of the overall chemical reaction and because the only means of water removal is

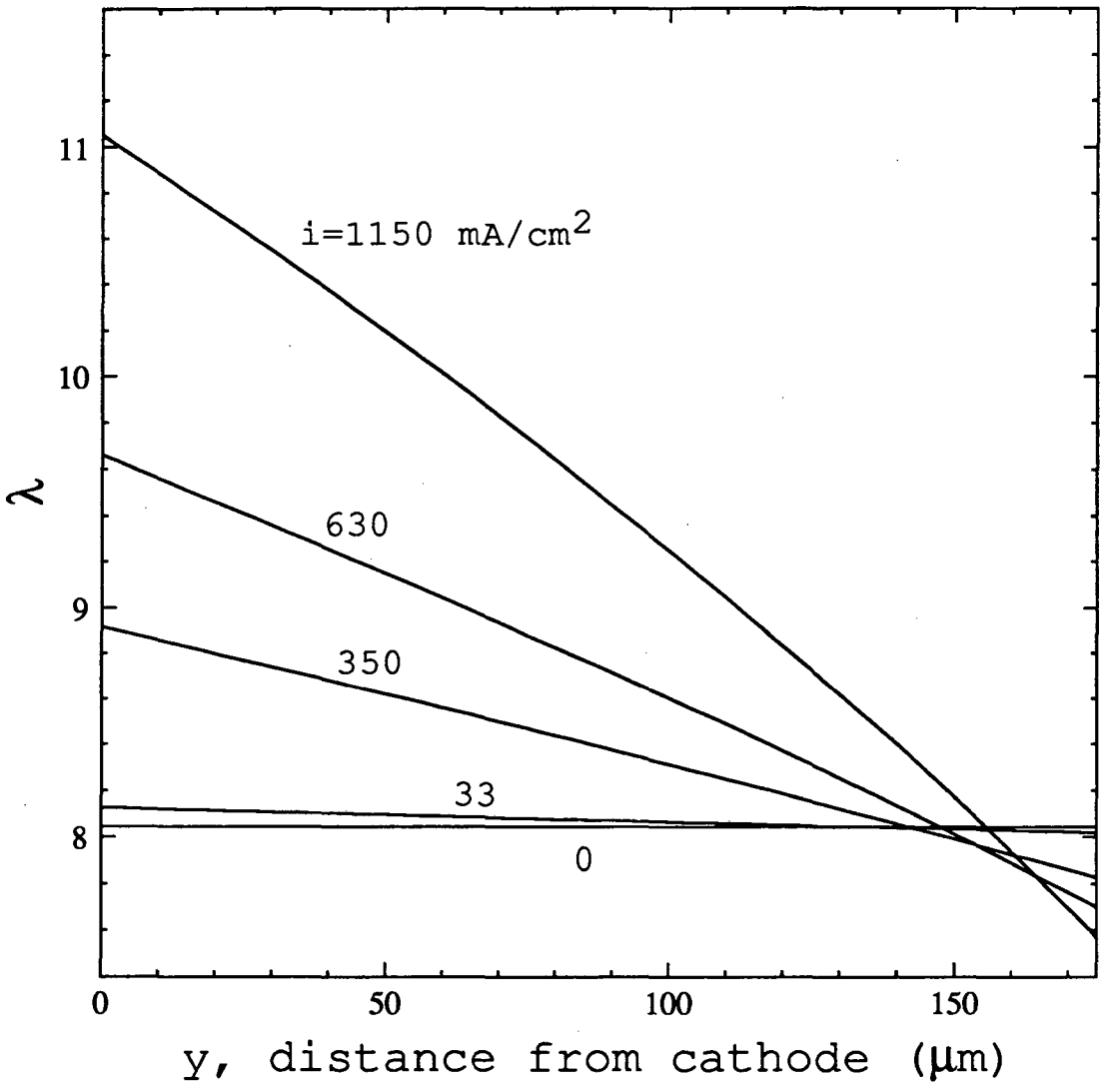


Figure 3. Water map for unit cell at various current densities. $p$=1.0 bar, $T$=353 K. Cathode is on the left; anode is on the right. $\lambda$ is the number of moles of water per sulfonic acid group.

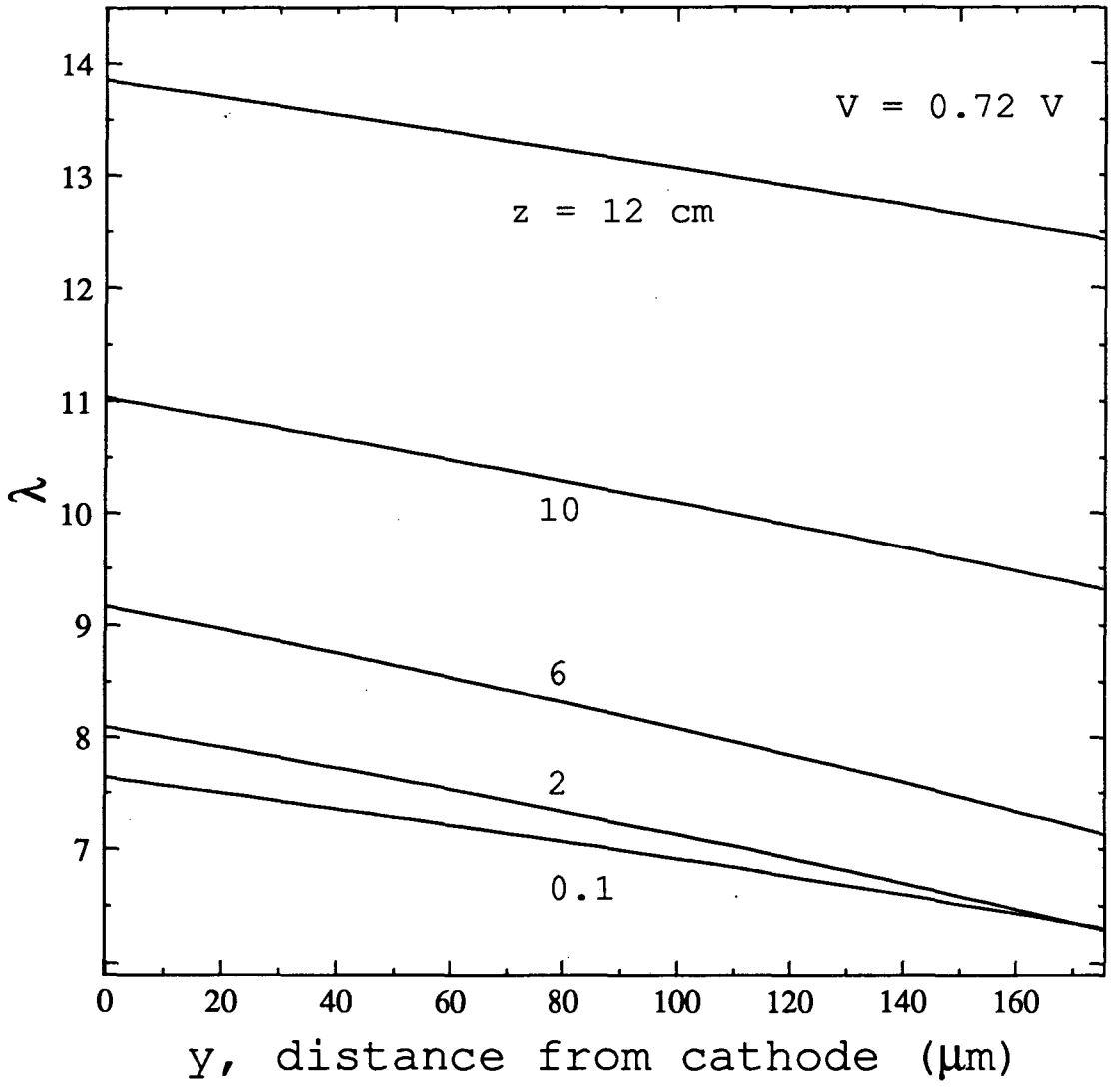


Figure 4. Concentration profiles of water across membrane. $\lambda$ is the number of water molecules per sulfonic acid group. $f$ = 1.0, $V$ = 0.72 volts, and $z$, the distance from the top of the channel, is a parameter.

Table 2.
Inlet gas composition.

| cathode-gas | | anode-gas | |
|---|---|---|---|
| $x_{H_2O}$ | 0.36 | $x_{H_2O}$ | 0.36 |
| $x_{N_2}$ | 0.512 | $x_{CO_2}$ | 0.16 |
| $x_{O_2}$ | 0.128 | $x_{H_2}$ | 0.48 |

| parameter | value |
|---|---|
| $T$ | 353.0 K |
| $L$ | 0.0175 cm |
| $p$ | 1.0 bar |
| $\epsilon_m$ | 0.20 |
| $\epsilon_g$ | 0.40 |
| $F_a^o$ | $1.0\times10^{-2}$ mol/m·s |

in the gas streams. Consequently, the level of hydration in the membrane increases with larger $z$. As before, there is a concentration gradient established that counteracts the electroosmotic drag of water and reduces the net transport of water across the cell.

The mole fractions of hydrogen, oxygen, and water as a function of axial position are shown in figure 5. The local current density is also depicted by the solid line in figure 5. At small $z$, there is a large net flux of water from the anode to the cathode gas stream. Consequently, the mole fraction of hydrogen is nearly constant for the first couple of centimeters. Initially the current density decreases; but as the membrane becomes more hydrated, the conductivity increases substantially, and the local current density rises.

Figure 6 shows the composition of water in the two gas streams. We have introduced the variables

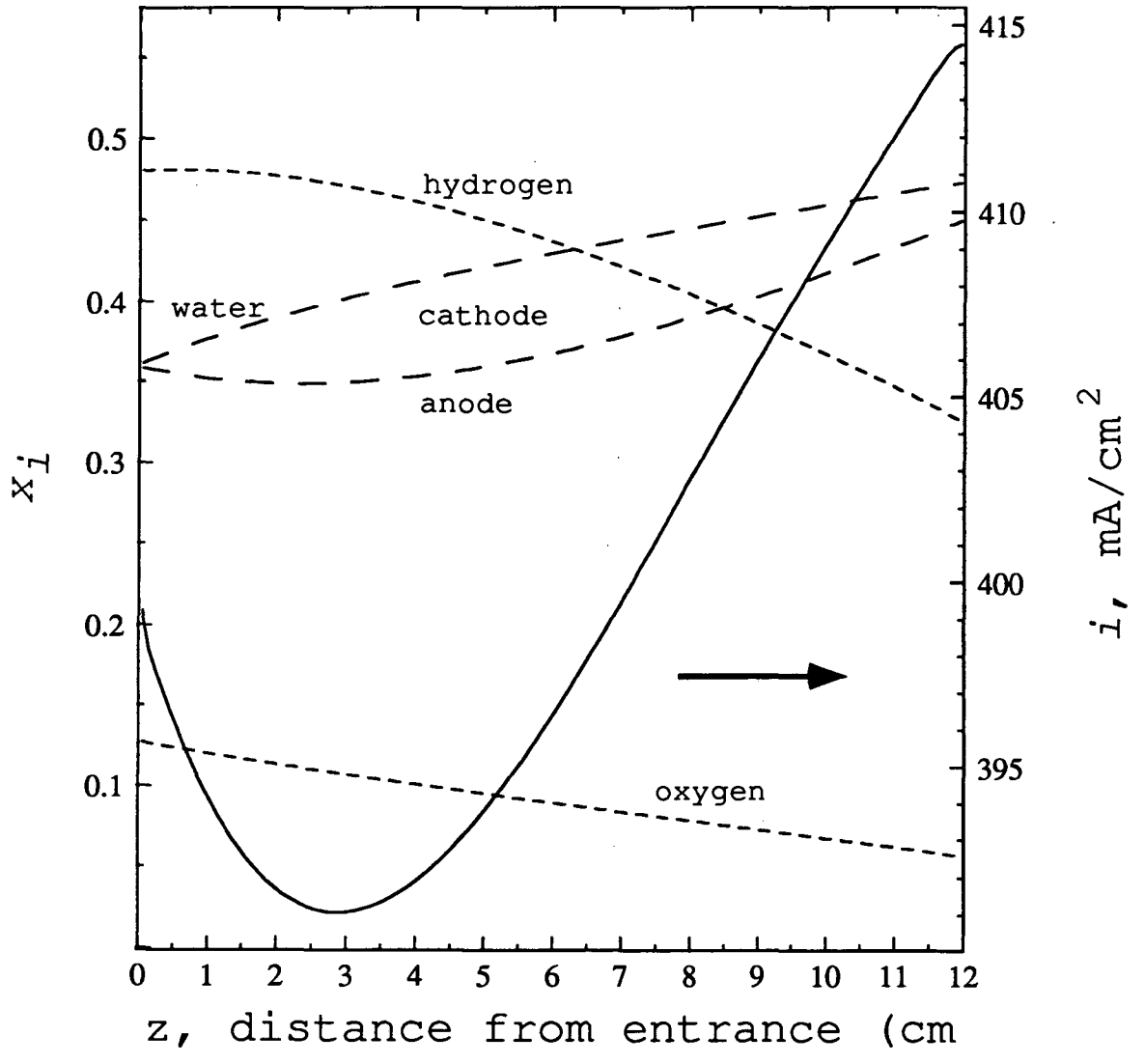


Figure 5. Mole fraction of hydrogen, oxygen, and water in the gas channels. Local current density is shown by the solid line. $V$=0.72 volts, and $f$=1.0.

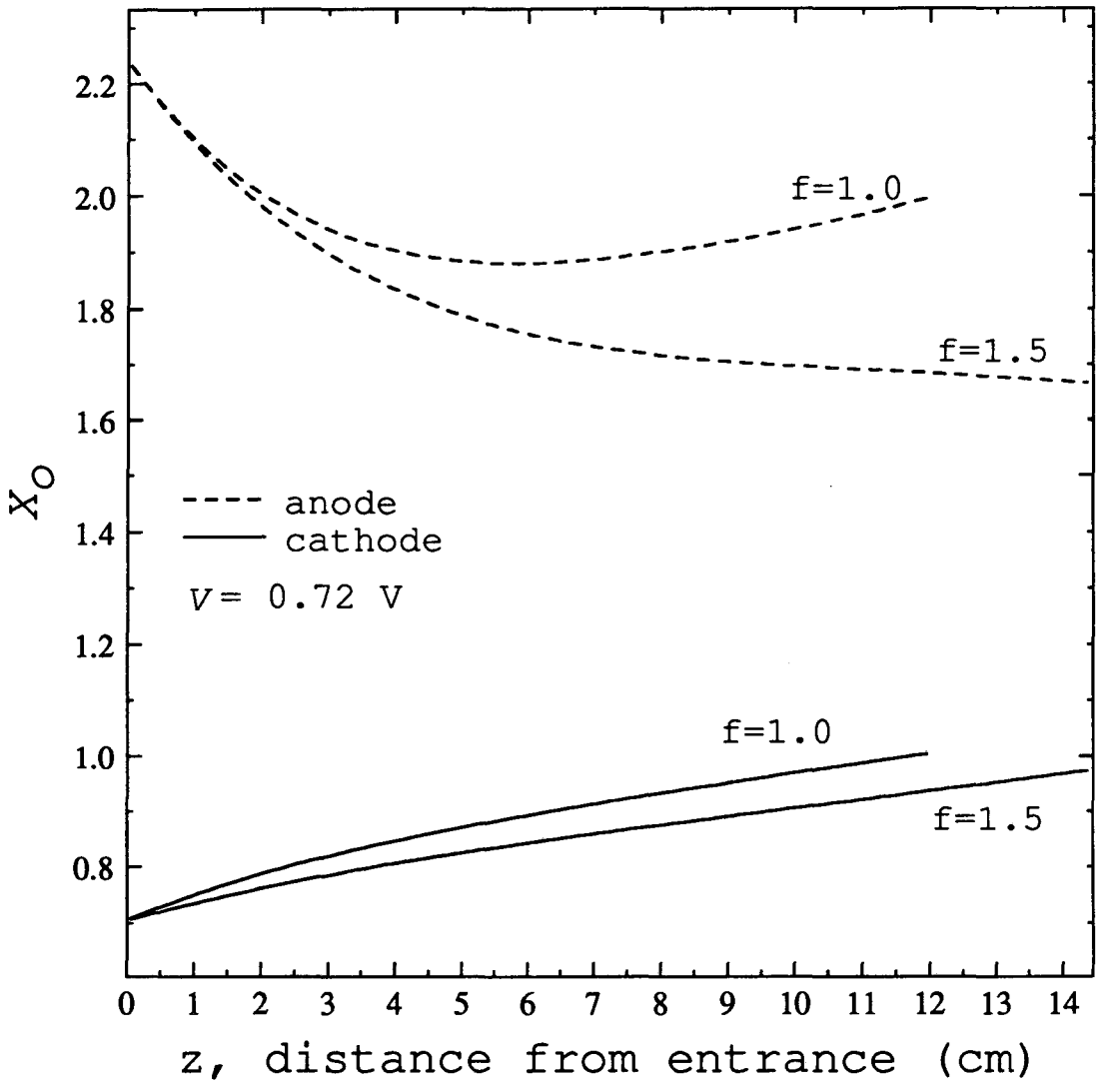


Figure 6. Composition of water in gas channels. $f$ is the air-to-fuel ratio. Simulation is stopped at the value of $z$ where the cathode gas stream reaches saturation with respect to water. Utilization of hydrogen is then 0.52 and 0.67 for $f$ = 1 and 1.5, respectively.

$$X_i = \frac{F_i}{F_{inert}} = \frac{x_i}{x_{inert}}, \tag{11}$$

where inert refers to the nonreacting gas in each stream: nitrogen for the cathode and carbon dioxide for the anode. $f$ is the molar flow rate of the cathode gas stream divided by the stoichiometric flow rate for a specified anode gas flow rate. The mole ratio of water in the cathode stream increases; and for $f$=1.5, the mole ratio in the anode stream decreases. For $f$=1, the composition of water in the anode stream goes through a minimum beyond which point water is being removed from both sides of the assembly (also see figure 8).

As the flow rate of air increases, one observes that: 1) the cell is able to operate longer before the cathode stream becomes saturated, 2) more water is removed in the cathode gas stream, and 3) the anode is further dehydrated. Thus, increasing air flow doesn't impact negatively on hydrogen utilization. The simulation was stopped when the cathode stream became saturated with water. For $f$=1 and $f$=1.5, this point corresponds to hydrogen utilization of 0.52 and 0.67, respectively.

In figure 7, the local superficial current density is plotted against local hydrogen utilization, with the cell potential as a parameter. The fractional utilization of hydrogen,

$$u = \frac{X^o_{H_2} - X_{H_2}}{X^o_{H_2}}, \tag{12}$$

is an important parameter in the optimization of a fuel cell.[21] With the potential of the two electrodes constant, one expects the current

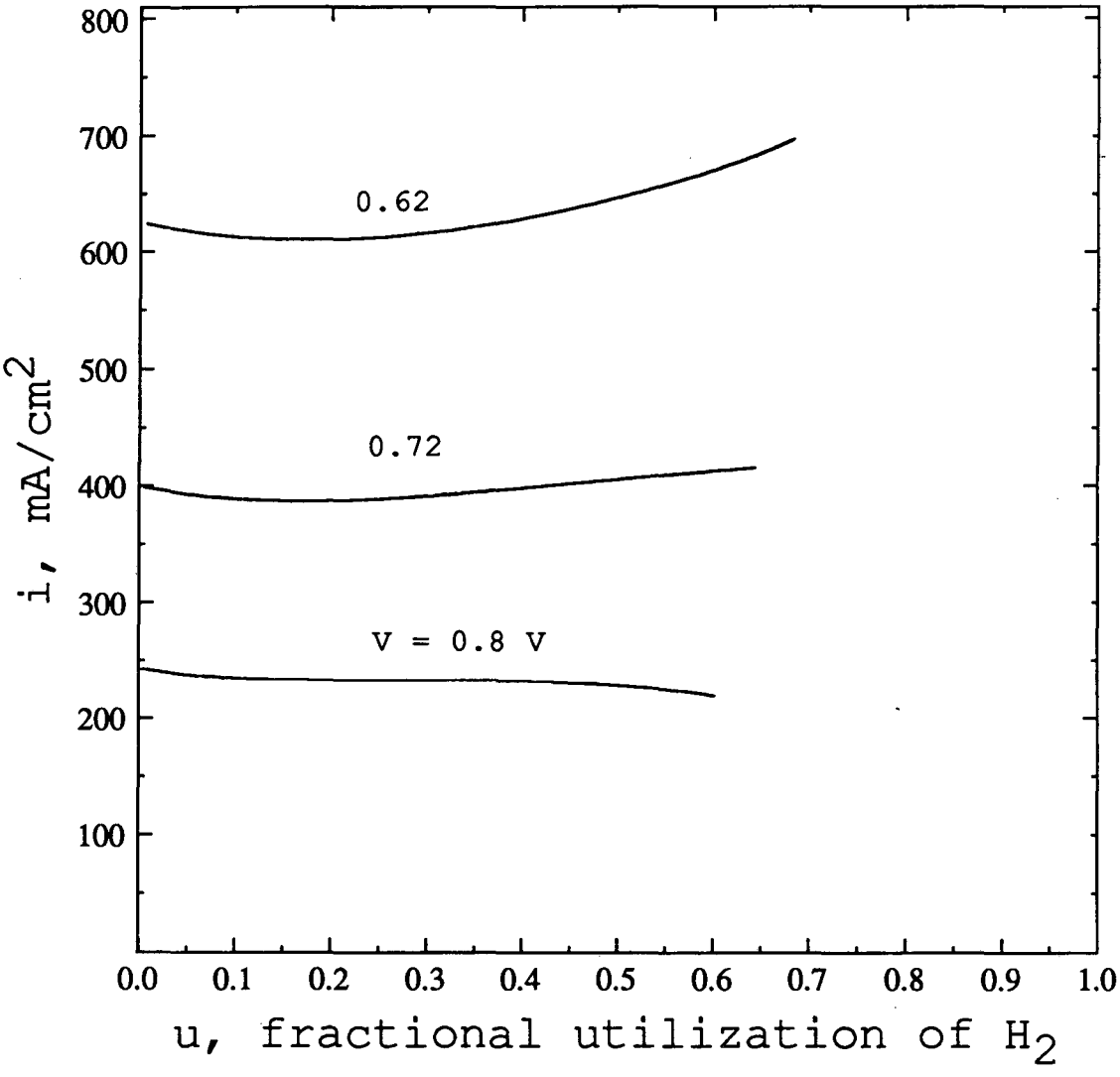


Figure 7. Local current density as a function of local utilization of hydrogen with *V*, the cell potential, as a parameter. $f$ = 1.5.

density to decrease as the reactants are consumed. Here, however, the conductivity increases dramatically with hydration of the membrane, and we observe an improvement in performance. At higher current densities, ohmic losses are more important, and consequently the improvement in performance is more dramatic. Since our model does not consider the condensation of water, we stop the simulation when the partial pressure of water equals the vapor pressure of the liquid, and we don't observe the utilization going to unity.

The net transport of water across the separator is shown in figure 8. At the top of the channel ($z$=0), the partial pressure of water is identical in the two gas channels, and consequently there is a large flux from the anode to the cathode due to the electroosmotic drag of water. Farther down the channel, the partial pressure of water in the cathode stream becomes greater than that of the anode, and the current density diminishes, thus lessening the net flux of water. With a large enough difference in partial pressure of water across the membrane, the flow of water can be reversed. This is seen in figure 8 at $z\approx6$ cm for $f$=1; beyond this point water is being removed from both sides.

Integrating in the $z$ direction we can calculate the ratio of moles of water transported across the cell to the moles of hydrogen ions passed. The ratio is 0.12 and 0.16 for $f$=1.0 and $f$=1.5 respectively. Because of the concentration gradient that counteracts the electroosmotic drag of water, these values are much lower than the transport number of water ($\approx$1). Nevertheless, raising the flow rate of air increases the net transport of water across the cell.

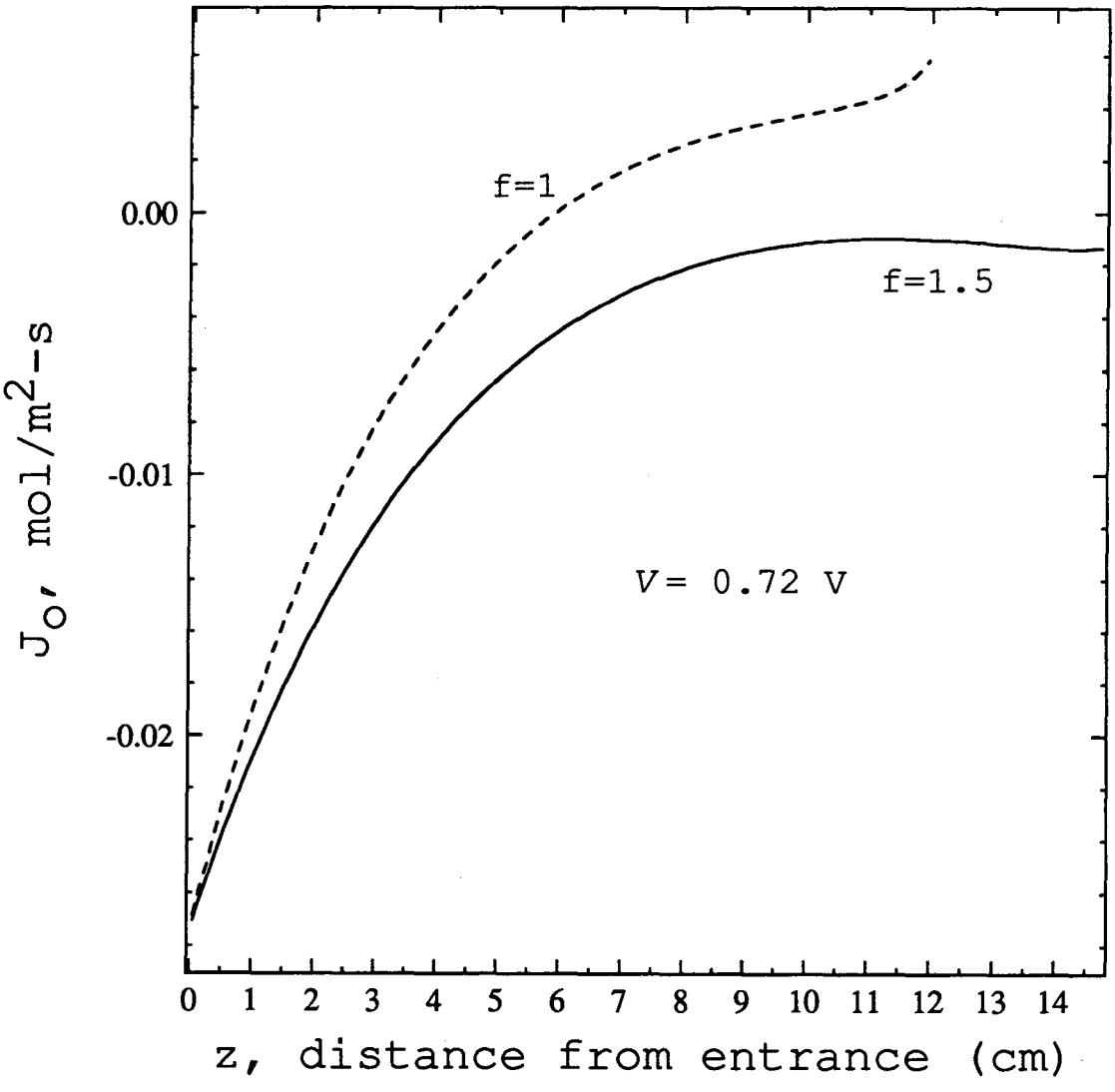


Figure 8. Net flux of water across membrane. A value of the flux less than zero indicates transport from the anode to the cathode. *f* is the air-to-fuel ratio. Simulation is stopped at the value of *z* where the cathode gas stream reaches saturation with respect to water.

Finally, we examine the heat transfer required to maintain constant temperature. There are significant losses and generation of heat. With $f$=1, $V$=0.72 V, and for the conditions of table 2, the following is calculated at $z$=10 cm.

| quantity | value |
|---|---|
| $F_T \Delta H$ | -0.5147 kW/m |
| $W$ | 0.3208 kW/m |
| $Q$ | -0.1939 kW/m |

The above calculations include the heat of vaporization of the product water. With an ambient temperature of of 298 K ($\Delta T$=55 K), the heat-transfer coefficient is estimated from equation 9 to be $h$=35.3 W/m$^2$·K. This is a typical value for forced convection of gases.[22]

From this isothermal analysis we are able to draw some conclusions. First, substantial heat removal is required to maintain the system at constant temperature. The temperature difference we used is large, and it seems impractical to increase this substantially. Thus at higher current densities, larger heat-transfer coefficients are needed. Second, there is significant transport of water from the anode to the cathode. Excess heat and water could be removed by passing air in excess of that required by stoichiometry; but this increases the net transport of water across the cell. Increasing the pressure of the air stream can be used to counteract the electroosmotic drag of water; nevertheless, this does not appear practical for transportation applications. Although the model is not able to simulate countercurrent flow of fuel and air streams, our results suggest that this could be helpful. Finally, we note that while the pressure drop in the $z$ direction would increase, the length of the assembly will scale linearly with increasing

flow rate.

*Nonisothermal Case.* — Temperature has a profound effect on equilibrium and kinetic properties. In this last section, we assumed that there are no temperature variations across the assembly (the $y$ direction) and that there is no transfer of heat in the $z$ direction. The temperature of the gases at the inlet is specified, and here we calculate the temperature in the $z$ direction based on an energy balance. Heat is removed by both an increase in temperature of the flowing gases and by heat transfer to an external medium at a temperature of 298 K.

Figure 9 shows water profiles across the membrane with $z$ as a parameter. The operating conditions are shown in table 2 but also include a heat-transfer coefficient of 30 $W/m^2 \cdot K$. The current density as a function of local utilization of hydrogen is shown in figure 10; the corresponding temperature profile is depicted in figure 11.

The hydration of the membrane is sensitive to the rate of heat removal. Because of the low thermal capacity of the gas streams, the steady-state temperature will rise quickly without adequate removal of heat. At even moderate current densities, the cell would dehydrate, and the performance would be poor.

In contrast to the isothermal water profiles of figure 4, for $h$=30 $W/m^2 \cdot K$, the temperature initially rises sharply with increasing axial distance, and water evaporates from the membrane (see figure 9). At constant cell potential, the loss of water from the membrane (and the consequent decrease in conductivity) results in lower current densities and the temperature levels off. Farther down the channel, the temperature decreases slowly, and the water content in the membrane increases

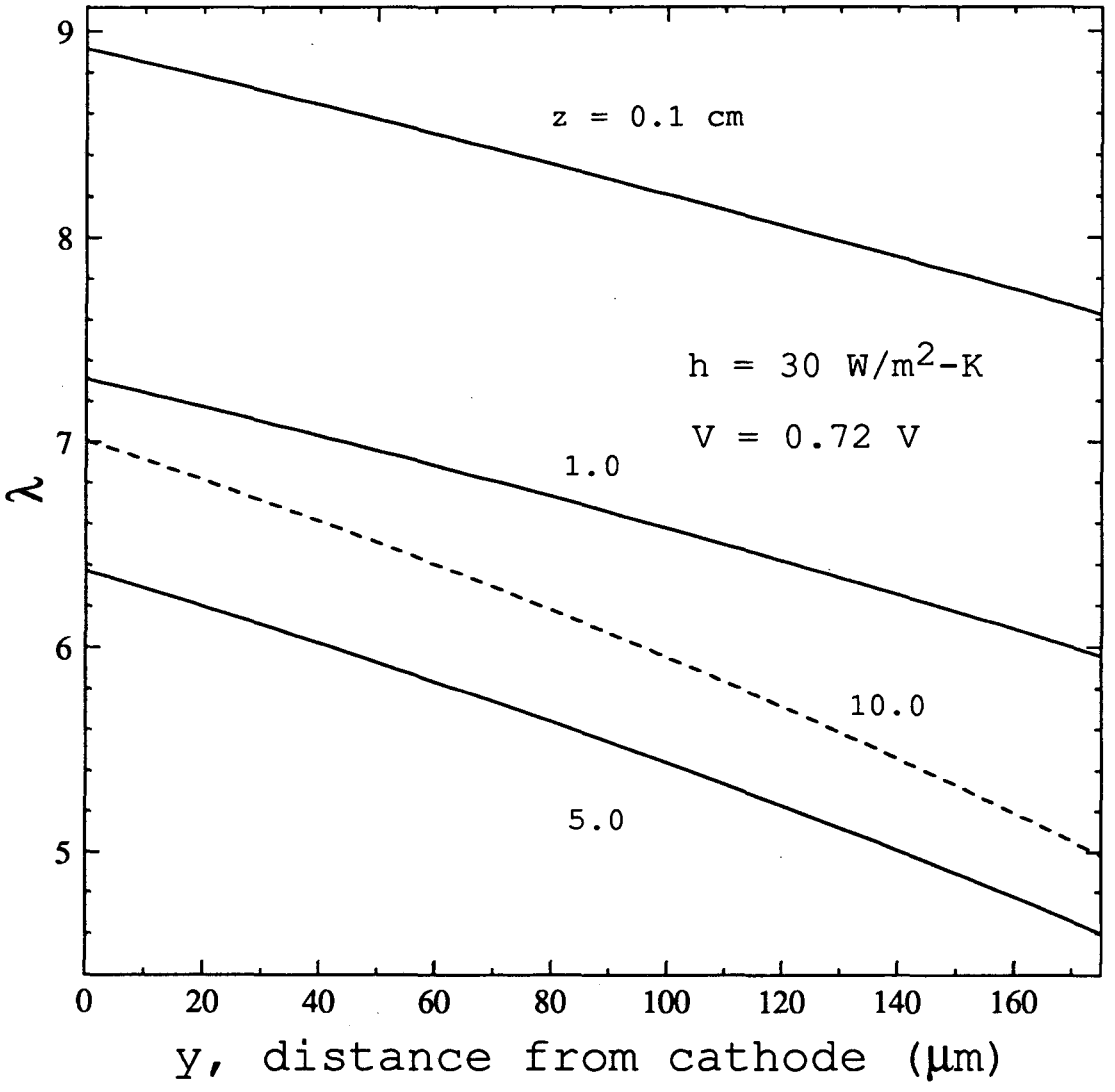


Figure 9. Concentration profiles of water across the membrane. $\lambda$ is the number of water molecules per sulfonic acid group. $V$=0.72 volts, and $z$, the distance from the top of the channel, is a parameter.

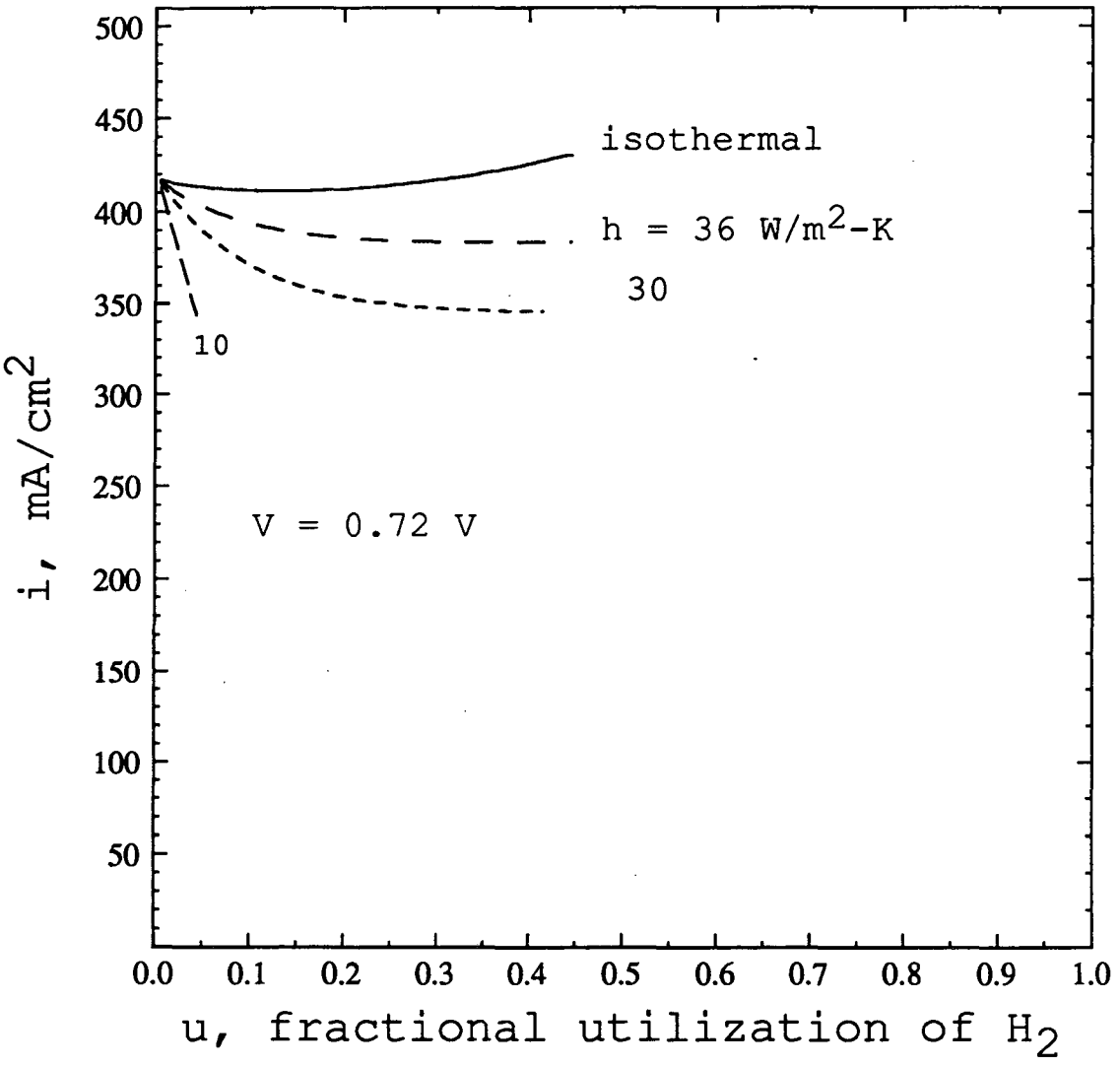


Figure 10. Local current density as a function of local utilization of hydrogen with *V*, the cell potential, fixed, and the heat-transfer coefficient as a parameter. $f = 1$.

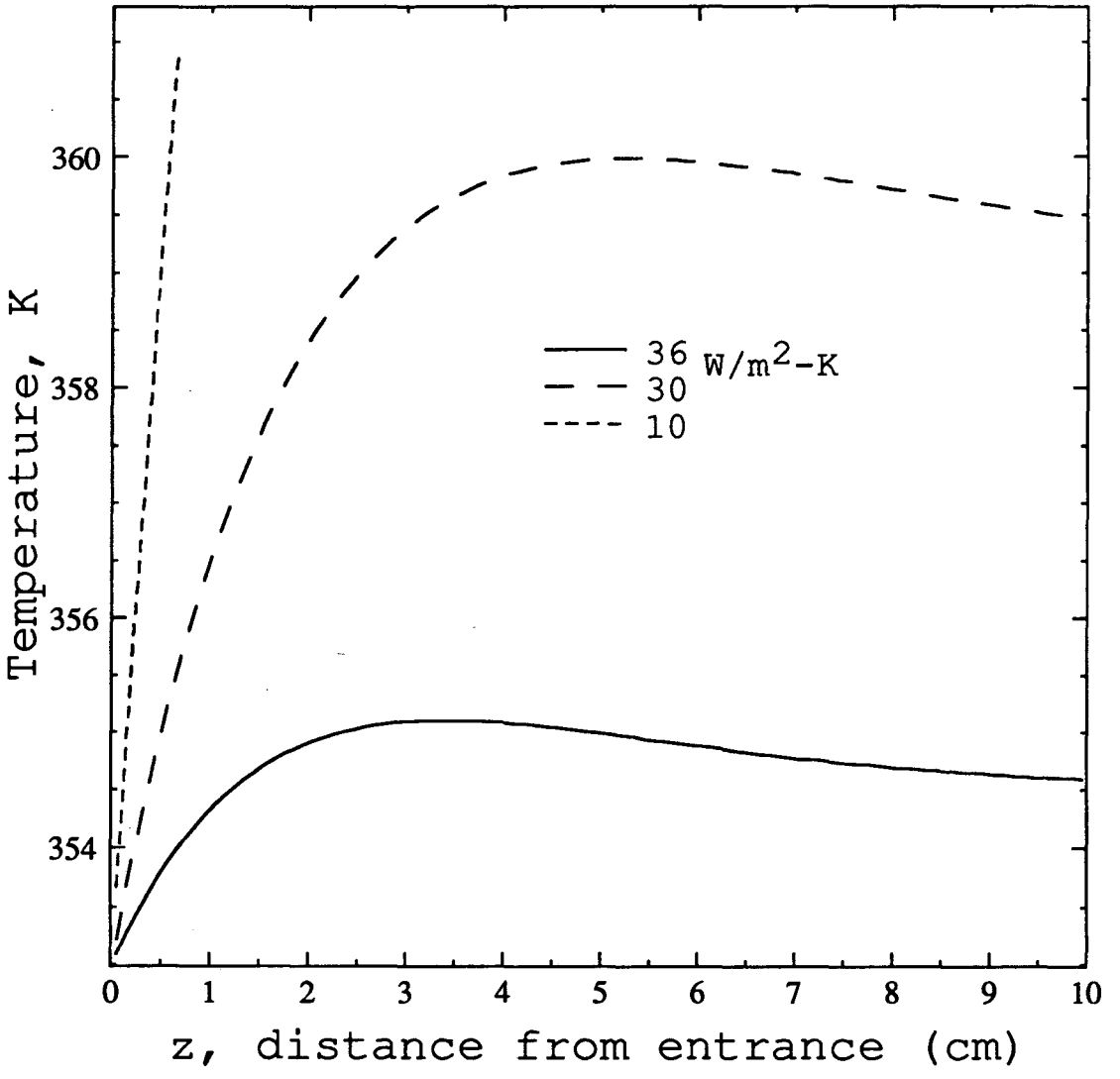


Figure 11. Temperature in gas channels. $f$ = 1 and $V$ = 0.72 V.

(see the dashed line in figure 9).

The effect of the heat-transfer coefficient on the performance is seen in figure 10. For $h$=36 W/m$^2$·K, the cell temperature rises slowly, and the performance is good. With a slightly lower value of the heat-transfer coefficient ($h$=30 W/m$^2$·K), the temperature increases more sharply, the membrane dehydrates, and the performance decreases substantially. With little or no removal of heat ($h$=10 W/m$^2$·K), the temperature rises more than 10°C in 1 cm, and there is a dramatic drop in the local current density.

It has been observed that the performance of these cells improves when gas streams saturated with water at a temperature above the operating temperature of the cell are used in the anode and cathode. This may be not so much because of the additional water supplied to the anode but rather because of improved heat transfer (dehydration of the membrane was not seen in the isothermal case). The evaporation of liquid water would result in a high heat-transfer coefficient, providing good temperature stability.

From the analysis of the energy balance, we conclude that thermal considerations must be included in an analysis of water management. Thermal control is critical to the performance of the solid-polymer-electrolyte fuel cell. The system is stable in the sense that high current density will result in high resistance. Nevertheless, the heat-transfer requirements will change markedly with current density, making temperature control more difficult.

## Acknowledgments

This work was supported by the Assistant Secretary for Conservation and Renewable Energy, Office of Transportation Technologies, Electric and Hybrid Propulsion Division of the U. S. Department of Energy under Contract No. DE-AC03-76SF00098.

## Appendix

Springer *et al.*[13] measured the electrical conductivity of Nafion® 117 membrane at various temperatures and water contents. The diffusion coefficient was estimated to be[16]

$$D_o = 3.5\text{x}10^{-2}\ \lambda\ \exp^{(-2436/T)}\ \text{cm}^2/\text{s}. \qquad \text{(A-1)}$$

The transport number of water was taken from reference 15.

The diffusion coefficients in the gas phase were estimated from kinetic theory. Assuming the ideal-gas law holds, Bird *et al.*[17] gave the approximate formula

$$D_{AB} = 0.0018583\ \frac{\sqrt{T^3\left(\frac{1}{M_A}+\frac{1}{M_B}\right)}}{p\sigma_{AB}^2\Omega_{AB}}. \qquad \text{(A-2)}$$

The parameters of equation A-2 were taken from Reid *et al.*[23] The effective diffusion coefficient depends on the porosity of the material. However, experimental results are usually necessary to quantify this relationship. Meredith and Tobias,[24] for example, studied the conductivity of porous media in detail. Since the porosity of the fuel-cell

assembly is not well characterized, the relationship is somewhat arbitrary, and for convenience we chose

$$D_i^{eff} = \epsilon\, D_i. \tag{A-3}$$

Zawodzinski *et al.*[25] measured the absorption isotherm of Nafion® 117 membrane at 30°C. This relation (water content *versus* activity) was assumed to hold for all temperatures. The vapor pressure of water was calculated from Antoine's correlation.

The enthalpy of the gas is

$$H = \sum_i^m n_i \bar{H}_i. \tag{A-4}$$

Assuming no enthalpy change on mixing and neglecting the effects of pressure, the partial molar enthalpy can be expressed as

$$\bar{H}_i^* = \bar{H}_i = \tilde{H}_i^*(T_r) + \int_{T_r}^{T} C_p dT, \tag{A-5}$$

and the heat capacity of the gas is

$$\tilde{C}_p^* = a + bT + \frac{c}{T^2}. \tag{A-6}$$

The values of the constants for our fuel-cell system are taken from Lewis and Randall.[26]

Ticianelli *et al.*[3] and Uribe *et al.*[27] have studied the kinetics of oxygen reduction in solid-polymer-electrolyte fuel cells. The reaction

is first order in oxygen concentration, and the cathodic transfer coefficient is unity. The exchange current density reported by Ticianelli is based on the superficial area of the electrodes. There is no clear way to differentiate between the kinetic rate constants and the specific interfacial area. Therefore, we adjusted *a* and the kinetic rate constants to approximate Ticianelli's current-voltage curve, and we required that the open-circuit potential be consistent with the thermodynamic value.

Recently, Parthasarathy *et al.*[28] investigated the temperature dependence of the electrode kinetics of oxygen reduction and expressed their results as

$$i_o = i_o(T_r)\ \exp\left[\frac{\Delta E}{R}\left(\frac{1}{T_r} - \frac{1}{T}\right)\right]. \qquad \text{(A-7)}$$

We used the activation energy they reported ($\Delta E$ = 73.2 kJ/mol) and variations in $U^\theta$ with temperature (from the Gibbs-Helmholtz equation) to account for the change in kinetic rate constants with temperature.

We assumed that the oxidation of hydrogen was fast and did not represent a significant overpotential for the fuel cell. The absorption/evaporation of water was also assumed to be fast.

## List of Symbols

| | |
|---|---|
| *a* | specific interfacial area, $m^2/m^3$ |
| *c* | total concentration, $mol/m^3$ |

| | |
|---|---|
| $c_i$ | concentration of species $i$, $mol/m^3$ |
| $C_p$ | molar heat capacity, J/mol·K |
| $d_i$ | driving force for transport of species $i$, $N/m^3$ |
| $D_i$ | diffusion coefficient, $m^2/s$ |
| $D_{ij}$ | binary interaction coefficient, $m^2/s$ |
| $f$ | air-to-fuel ratio |
| $F$ | Faraday's constant, 96,487 C/eq |
| $F_a$ | molar flow rate of anode gas stream per unit width, mol/s·m |
| $F_T$ | total molar flow rate of gas per unit width, mol/s·m |
| $h$ | heat-transfer coefficient, $W/m^2 \cdot K$ |
| $H$ | enthalpy, J/mol |
| $i$ | current density, $A/cm^2$ |
| $i_o$ | exchange current density, $A/cm^2$ |
| $j_{in}$ | pore wall flux of species $i$, $mol/m^2 \cdot s$ |
| $J_i$ | molar flux in $y$ direction of species $i$, $mol/cm^2 \cdot s$ |
| $K_{ij}$ | frictional coefficient, $J \cdot s/m^5$ |
| $L$ | thickness of separator, cm |
| $M_i$ | molar mass of species $i$, g/mol |
| $n$ | number of species |
| $n_i$ | moles of species $i$, mol |
| $p$ | pressure, bar |
| $q$ | rate of heat transfer per unit area, $W/m^2$ |
| $Q$ | rate of heat transfer per unit width, W/m |
| $R$ | universal gas constant, 8.3143 J/mol·K |
| $T$ | temperature, K |
| $u$ | utilization of hydrogen |

| | |
|---|---|
| $v_i$ | velocity of species $i$, m/s |
| $V$ | cell potential, V |
| $W$ | work done by system per unit width, W/m |
| $x_i$ | mole fraction of species $i$ |
| $X_i$ | composition variable defined in equation 11 |
| $y$ | distance across membrane, cm |
| $z$ | distance from top of channel, cm |
| $z_i$ | charge number of species $i$ |
| $\epsilon$ | porosity of electrode |
| $\sigma_{AB}$ | characteristic length, nm |
| $\lambda$ | ratio of $H_2O/R\text{-}SO_3H$ |
| $\mu_i$ | electrochemical potential of species $i$, J/mol |
| $\Phi$ | electrical potential, V |
| $\Omega$ | diffusion collision integral |

Subscripts

| | |
|---|---|
| A | ambient temperature |
| g | gas phase |
| $\ell$ | electrolyte phase |
| o | water |
| r | reference state |
| + | hydrogen ion |

Superscripts

| | |
|---|---|
| * | ideal gas |
| ~ | per mole |

| | |
|---|---|
| – | partial molar quantity |
| o | inlet condition |

## References

[1] K. Prater, "The Renaissance of the Solid-Polymer Fuel Cell," *J. Power Sources*, **29**, 239-250 (1990).

[2] M. S. Wilson and S. Gottesfeld, "High Performance Catalyzed Membranes of Ultra-low Pt Loading for Polymer Electrolyte Fuel Cells," *J. Electrochem. Soc.*, **139**, L28-30 (1992).

[3] E. A. Ticianelli, C. R. Derouin, and S. Srinivasan, "Methods to Advance Technology of Proton Exchange Membrane Fuel Cells," *J. Electrochem. Soc.*, **135**, 2209-2214 (1988).

[4] J. Leddy and E. Vanderborgh, "Modeling of the Electrode/Ionomer Interface," in *Diaphragms, Separators, and Ion-exchange Membranes*, edited by J. W. Van Zee, R. E. White, K. Kinoshita, and H. S. Burney, proceedings volume 86-13, The Electrochemical Society, Pennington, N. J. (1986).

[5] *Fuel Cells*, edited by W. Mitchell, Academic Press, New York (1963).

[6] J. Giner and C. Hunter, "The Mechanism and Operation of the Teflon-Bonded Gas Diffusion Electrode: A Mathematical Model," *J. Electrochem. Soc.*, **116**, 1124-1130 (1969).

[7] *Handbook of Fuel Cell Technology*, edited by C. Berger, Prentice Hall, Englewood Cliffs, N. J. (1968).

[8] T. Nguyen, J. C. Hedstrom, and N. E. Vanderborgh, "Heat and Mass Transfer Design Issues in PEM Fuel Cell Hardware," *Proceedings of the Symposium on Fuel Cells*, edited by R. E. White and A. J. Appleby, proceedings volume 89-14, The Electrochemical Society, Pennington, N. J. (1989).

[9] Michael C. Kimble and Ralph White, "A Mathematical Model of a Hydrogen/Oxygen Alkaline Fuel Cell," *J. Electrochem. Soc.*, **138**, 3370-3382 (1991).

[10] Dawn M. Bernardi, "Water-Balance Calculations for Solid-Polymer-Electrolyte Fuel Cells," *J. Electrochem. Soc.*, **137**, 3344-3350 (1990).

[11] Dawn M. Bernardi and Mark Verbrugge, "Mathematical Model of Gas Diffusion Electrode Bonded to a Polymer Electrolyte," *AIChE J.*, **37**, 1151-1163 (1990).

[12] Dawn M. Bernardi and Mark Verbrugge, "Mathematical Model of the Solid-Polymer-Electrolyte Fuel Cell," *J. Electrochem. Soc.*, (submitted) GMR-7360.

[13] T. E. Springer, T. A. Zawodzinski, and S. Gottesfeld, "Polymer Electrolyte Fuel Cell Model," *J. Electrochem. Soc.*, **138**, 2334-2342 (1991).

[14] Thomas F. Fuller and John Newman, "A Concentrated Solution Theory Model of Transport in Solid-Polymer-Electrolyte Fuel Cells," *Proceedings of the Symposium on Fuel Cells*, edited by R. E. White and A. J. Appleby, proceedings volume 89-14, The Electrochemical Society, Pennington, N. J. (1989).

[15] Thomas F. Fuller and John Newman, "Experimental Determination of the Transport Number of Water in Nafion 117 Membrane," *J. Electrochem. Soc.*, 139, 1332-1337 (1992).

[16] Thomas F. Fuller, *Solid-polymer-electrolyte Fuel Cells*, Ph.D. Thesis, University of California, Berkeley, California (1992).

[17] R. Byron Bird, Warren E. Stewart, and Edwin N. Lightfoot, *Transport Phenomena*, John Wiley & Sons, Inc., New York (1960).

[18] John Newman, *Electrochemical Systems*, Prentice-Hall, Englewood Cliffs, N. J. (1991).

[19] D. Bernardi, E. Pawlikowski, and John Newman, "A General Energy Balance for Battery Systems," *J. Electrochem. Soc.*, 132, 5-12 (1985).

[20] Bernard Tribollet and John Newman, "Impedance Model for a Concentrated Solution," *J. Electrochem. Soc.*, 131, 2780 (1984).

[21] John Newman, "Optimization of Potential and Hydrogen Utilization in an Acid Fuel Cell," *Electrochim. Acta*, 24, 223-229 (1979).

[22] F. P. Incropera and D. P. DeWitt, *Fundamentals of Heat Transfer*, John Wiley & Sons, New York (1981).

[23] Robert C. Reid, John M. Prausnitz, and Thomas K. Sherwood, *The Properties of Gases and Liquids*, McGraw Hill (1977).

[24] R. E. Meredith and C. W. Tobias, "Conduction in Heterogeneous Systems," *Advances in Electrochemistry and Electrochemical Engineering 2*, C. W. Tobias, ed., Interscience Publishers, New York (1962).

[25] T. Zawodzinski, M. Neeman, L. Sillerud, and S. Gottesfeld, "Determination of Water Diffusion Coefficients in Perfluorosulfonated Ionomeric Membranes," *J. Phys. Chem.*, 95, 6040-6044 (1991).

[26] G. N. Lewis and M. Randall, revised by K. S. Pitzer and L. Brewer, *Thermodynamics*, McGraw-Hill Inc., New York (1961).

[27] F. A. Uribe, T. E. Springer, and S. Gottesfeld, "A Microelectrode Study of Oxygen Reduction at the Platinum Recast Nafion Film Interface," *J. Electrochem. Soc.*, 139, 764-773 (1992).

[28] A. Parthasarathy, S. Srinivasan, A. J. Appleby, and C. R. Martin, "Temperature Dependence of the Electrode Kinetics of Oxygen Reduction at the Platinum/Nafion® Interface - A Microelectrode Investigation," *J. Electrochem. Soc.*, in press (1992).

LAWRENCE BERKELEY LABORATORY
UNIVERSITY OF CALIFORNIA
TECHNICAL INFORMATION DEPARTMENT
BERKELEY, CALIFORNIA 94720